Recent Demographic History Inferred by High-Resolution Analysis of Linkage Disequilibrium

Enrique Santiago,*,[1] Irene Novo,[2] Antonio F. Pardiñas,[3] María Saura,[4] Jinliang Wang,[5] and Armando Caballero[2]

[1]Departamento de Biología Funcional, Facultad de Biología, Universidad de Oviedo, Oviedo, Spain

[2]Centro de Investigación Mariña, Departamento de Bioquímica, Genética e Inmunología, Edificio CC Experimentais, Campus de Vigo, Universidade de Vigo, Vigo, Spain

[3]MRC Centre for Neuropsychiatric Genetics and Genomics, Division of Psychological Medicine and Clinical Neurosciences, School of Medicine, Cardiff University, Cardiff, United Kingdom

[4]Departamento de Mejora Genética Animal, INIA, Madrid, Spain

[5]Institute of Zoology, Zoological Society of London, London, United Kingdom

*Corresponding author: E-mail: esr@uniovi.es.

Associate editor: Yuseob Kim

Abstract

Inferring changes in effective population size (N_e) in the recent past is of special interest for conservation of endangered species and for human history research. Current methods for estimating the very recent historical N_e are unable to detect complex demographic trajectories involving multiple episodes of bottlenecks, drops, and expansions. We develop a theoretical and computational framework to infer the demographic history of a population within the past 100 generations from the observed spectrum of linkage disequilibrium (LD) of pairs of loci over a wide range of recombination rates in a sample of contemporary individuals. The cumulative contributions of all of the previous generations to the observed LD are included in our model, and a genetic algorithm is used to search for the sequence of historical N_e values that best explains the observed LD spectrum. The method can be applied from large samples to samples of fewer than ten individuals using a variety of genotyping and DNA sequencing data: haploid, diploid with phased or unphased genotypes and pseudohaploid data from low-coverage sequencing. The method was tested by computer simulation for sensitivity to genotyping errors, temporal heterogeneity of samples, population admixture, and structural division into subpopulations, showing high tolerance to deviations from the assumptions of the model. Computer simulations also show that the proposed method outperforms other leading approaches when the inference concerns recent timeframes. Analysis of data from a variety of human and animal populations gave results in agreement with previous estimations by other methods or with records of historical events.

Key words: effective population size, genetic drift, demography, SNP, ancient DNA.

Introduction

Several models and sophisticated mathematical tools have been developed to extract demographic information from the rapidly growing amount of genomic data. These models focus on different aspects of the genetic variability generated by mutation and recombination. When recombination is not considered, the only free parameter is the mutation rate, which becomes the metronome of the coalescence process (Hudson 1990). Because mutations accumulate slowly, these models are suitable for estimating the effective population size (N_e) from very ancient times (Atkinson et al. 2008) with the limit given by the coalescence time of all the sequences in the sample. The inclusion of recombination reflects better the reality of nuclear genomes and improves the estimations of past N_e not only for more recent times but also for distant times as several genome segments can be considered in the same analysis (Li and Durbin 2011; Schiffels and Durbin 2014;

Palacios et al. 2015; Terhorst et al. 2017; Speidel et al. 2019). However, the role of mutation remains central in the estimation of the lengths of genealogy branches and the impact of recombination is restricted to a small genomic scale. With fairly accurate estimates of N_e in the ancient past of several thousands of generations, these methods are not expected to provide good estimates for very recent timeframes (say, within 200 generations).

Models based exclusively on the theory of linkage disequilibrium (LD) between loci measure the time by the rate of occurrence of recombination events, which can take values several orders larger than mutation rates when loci are distant. Thus, the particular rate of mutation becomes irrelevant and the inference of population sizes from LD concerns essentially the recent demographic history, which is key to understand the current genetic composition of small populations. To some extent, the structure of LD of a

population can be described by the distribution of tracts of identity by descent (IBD) and the recent demography can be inferred from this distribution by the principle that longer tracts shared by individuals correspond to more recent common ancestors and thus imply smaller N_e in the more recent past (Hayes et al. 2003; Palamara et al. 2012; Browning and Browning 2015). However, only long IBD tracts, which are infrequent in small samples from large populations, can be reliably identified. Thus, large samples of phased genotypes are usually needed in order to reach some resolution for a general trend of demography.

A simplified representation of the structure of LD is given by the correlation between alleles of pairs of loci (Sved and Hill 2018). Two locus statistics provide additional power over one locus statistics in recovering past demography (Ragsdale and Gutenkunst 2017). This basic theory has proven to be useful for estimating the current N_e of small populations from LD between unlinked loci (Waples 2006; Waples and Do 2008; Sved et al. 2013; Wang et al. 2016) and has also been extended to infer changes in N_e in the recent past from LD between linked loci (Hayes et al. 2003; Tenesa et al. 2007; Qanbari et al. 2010; Corbin et al. 2012; Mörseburg et al. 2016). The fundamental idea is that LD between pairs of SNPs at different genetic distances provides differential information on N_e at different time points in the past.

Several methods assume that the expected LD between loci at a particular recombination rate is the result of genetic drift at a particular generation (Barbato et al. 2015; Mezzavilla and Ghiroto 2015; Hollenbeck et al. 2016). By assuming that the observed LD between loci pairs at a genetic distance $1/(2t)$ Morgans reflects the N_e value t generations back in time, they are able to estimate general trends with slow changes in population size, which is a remarkable achievement for a rather simplistic approach. However, although LD for closely linked loci depends more strongly on genetic drift occurred far in the past than LD for loosely linked loci, the magnitude of LD between loci at any given genetic distance is the result of the cumulative effects of genetic drift (determined by N_e^{-1}, which generates LD) and recombination (determined by genetic distance, which reduces LD) occurred over all the previous generations.

Here, we derive equations for the expected contributions of each of the past generations to the LD of pairs of loci separated by a particular genetic distance. We also develop corrections for the sampling effects (i.e., LD due to finite sample size), covering the most general types of SNP data from both genotyping and DNA sequencing: diploid unphased genotypes, diploid phased genotypes and pseudohaploid genotypes of low-coverage genomes usually resulting from sequencing ancient DNA (Haak et al. 2015). Based on the principle that the observed LD for different genetic distances provides differential information of past N_e at different generations, we develop an optimization method (genetic optimization for N_e estimation [GONE]) that implements a genetic algorithm (Mitchell 1998) to infer the recent demographic history of a population from SNP data of a small sample of contemporary individuals. The method is validated by simulation under different demographic scenarios, and is

compared with the previous leading methods, MSMC (Schiffels and Durbin 2014), Relate (Speidel et al. 2019), and the algorithms used by previous LD-temporal N_e methods, such as SNeP (Barbato et al. 2015), NeON (Mezzavilla and Ghiroto 2015), or LinkNe (Hollenbeck et al. 2016). We next inferred the historic population sizes from a number of real data sets from animal and human populations.

Results

Theoretical Developments

We derived the expectations for the squared covariance between the alleles of a given pair of loci (D^2) and the product of their two variances (W), such that the LD between the loci is measured by the standardized quantity $\delta^2 = E[D^2]/E[W]$ (Ohta and Kimura 1969) (see Supplementary File, Supplementary Material online).

Constant Effective Population Size

When population size is kept constant over generations, the expected values $E[D^2]$ and $E[W]$ in consecutive generations can be obtained by considering a third statistic $E[D(1-2p)(1-2q)]$, where p and q are the allele frequencies at both loci (Hill and Robertson 1968; Hill 1975). This third statistic is equivalent to the moment of order (2,2)th that we approximate in terms of D^2 and W by assuming that most of the new LD produced at any generation is built by drift acting on old variation (see Appendix in Supplementary File, Supplementary Material online).

At equilibrium, after many generations with constant effective population size N_e, constant mutation rate and recombination rate c, δ^2 can be predicted by N_e and c as:

$$\delta_c^2 = \frac{1 + c^2 + N_e^{-1}}{2N_e\left(1 - (1-c)^2\right) + 2.2(1-c)^2} \quad . \quad (1)$$

Note that δ^2 is, in fact, the squared correlation coefficient $r^2 = D^2/W$ (Hill and Robertson 1968) weighted by the product of variances, that is, $\delta^2 = E[r^2W]/E[W]$ (Rogers 2014). Under simplified assumptions (negligible c^2 and N_e^{-1}), equation (1) is close to the classical Sved's (1971) approximation, $r^2 \approx 1/[4N_ec + 2]$, for the case of unknown phase. Equation (1) is valid for the whole range of c values. For independent loci ($c = \frac{1}{2}$) and neglecting the term N_e^{-1}, equation (1) is simplified to $5/(6N_e)$. Likewise, the corresponding equation for haploid genomes (eq. S2 in Supplementary File, Supplementary Material online) reduces to $2/(3N_e)$. The quantitative difference between δ^2 and r^2 has been considered typically small, particularly for intermediate allele frequencies. However, important biases in the estimation of N_e could be found if r^2 instead of δ^2 is used (supplementary fig. S1, Supplementary Material online).

In practice, sampling could also generate LD (equivalent to one extrageneration of recombination and drift) and thus its effects need to be corrected to obtain the estimate of population (rather than sample) δ^2. Approximate corrections for several data types (haploids, phased diploids, unphased

diploids, and pseudohaploid genomes) are given in the Supplementary File, Supplementary Material online.

Variable Effective Population Size

When population size changes with time, the above equation for δ^2 does not hold and the historical series of N_e cannot be inferred from a single δ^2 value. For a particular recombination rate (c), the expectation of the current D_c^2 can be expressed as:

$$E\left[D_c^2\right] \approx \sum_{g=0}^{\infty}(C_g \cdot 2N_g\mu),$$

where C_g (Section 10 of Supplementary File, Supplementary Material online) is the contribution to the current squared covariance of a single mutation occurred at generation g back in time and the term $2N_g\mu$ is the number of new mutations at that generation, N_g being the effective population size N_e at generation g and μ the mutation rate that is assumed to be constant across loci and generations.

In the same way, $E[W_c]$ can be expressed as:

$$E[W_c] = \sum_{g=0}^{\infty}(w_g \cdot 2N_g\mu) \approx \mu \sum_{g=0}^{\infty}\left[V_x \cdot \prod_{i=0}^{g-1}\left(1 - \frac{1}{N_i}\right)\right],$$

where w_g is the contribution to the current product of variances from a mutation occurred at generation g, and V_x is the background neutral variance. The factors with negative index i equal 1. Note that the expression in the right-hand side shows the decline in genetic variation by genetic drift. The ratio of expectations $E\left[D_c^2\right]$ and $E[W_c]$ for a particular recombination value c becomes independent of μ,

$$\delta_c^2 = \frac{E\left[D_c^2\right]}{E[W_c]} = \frac{\sum_{g=0}^{\infty}(C_g \cdot 2N_g)}{\sum_{g=0}^{\infty}\left[V_x \cdot \prod_{i=0}^{g-1}\left(1 - \frac{1}{N_i}\right)\right]}.$$

An estimate of the temporal series of N_g values can be obtained from the observed δ_c^2 values for pairs of markers with different recombination rates c. Consequently, we developed a genetic algorithm implemented into a computer program (GONE) to search for the temporal N_g values that minimize the sum of squares of the difference between the expected and observed δ_c^2 values (see Materials and Methods). Supplementary figure S2, Supplementary Material online, shows the close agreement between the observed and optimized values of δ_c^2 for different demographic scenarios.

Simulation Results

Over 10^8 replicates were simulated for each combination of recombination rate and population size in order to check the accuracy of the predictions of δ^2 for constant population sizes for diploids (eq. 1) and haploids (eq. S2 in Supplementary File, Supplementary Material online). The predictions turned out to be very close to simulations over the whole range of recombination rates (supplementary table S1 and fig. S3,

Supplementary Material online). They are accurate even at the two boundaries of the range of recombination rates $c = 0.5$ and $c = 0$, where the true δ^2 value used to be controversial. Both table and figure also show predictions by other methods.

We evaluated GONE for the ability to infer the true historic series of N_e values of simulated populations. Inferences were carried out from LD data between loci with recombination rates from 0.001 to 0.5. Several profiles of changes in population size were simulated, and the resulting genetic data were analyzed by GONE in comparisons with three of the leading methods, MSMC (Schiffels and Durbin 2014), Relate (Speidel et al. 2019), and the algorithms used by the previous LD-temporal N_e methods (such as SNeP, NeON, or LinkNe). The results are shown in figure 1 for a representative sample of demographic scenarios. Within the range of the most recent 200 generations, GONE outperforms the other methods, which are, at most, able to detect a general trend for both phased and unphased data. The previous simple LD-temporal N_e approach performs fairly well when compared with Relate and MSMC, particularly for unphased data. Relate is prone to large estimation errors in recent generations, which suggests that coalescence methods are better suited for ancient N_e estimations.

Figure 2 illustrates different characteristics of the estimations by GONE. First, the accuracy of the estimations decreases with time: Ancient demographic changes, like a bottleneck at generation 140 in the figure (fig. 2B), are detected with lower precision than recent ones (fig. 2A). Second, overlapping generations cause some underestimations in the recent generations (fig. 2C). Third, the inferences from synthetic populations created by mixing several populations in past times do not show distortions in N_e estimations from the time mixing to present (fig. 2D). Fourth, no distortion or bias occurs when the analysis deals with metapopulations structured according to the standard island model, and the migration rate between subpopulations is high (fig. 2E). The estimates correspond to the total size of the metapopulation, in agreement with the expected effective population size from the classical N_e theory. However, there are substantial biases in the estimates for recent generations when the migration rate is low (fig. 2F). Fifth, base-calling errors do not affect estimates in a significant way if they are not larger than 1%, which is a reasonable assumption for data from common commercial genotyping and sequencing platforms (fig. 2G). Other methods need high-quality sequences or the application of a threshold MAF to eliminate the distortion caused either on genealogies or on correlations between alleles at different loci. Sixth, the sampling of non-contemporary individuals causes a bias in the estimations of the most recent generations (fig. 2H). This scenario assumes that each of the individuals are sampled in each of the last 100 generations. The distortion in these estimates seems to be significant but affecting a time of inference which is smaller (about a quarter) than the length of the sampling period. Finally, the random selection of individuals of a small sample leads to differences in the estimations from different samples, particularly for the most recent generations (fig. 2I). These
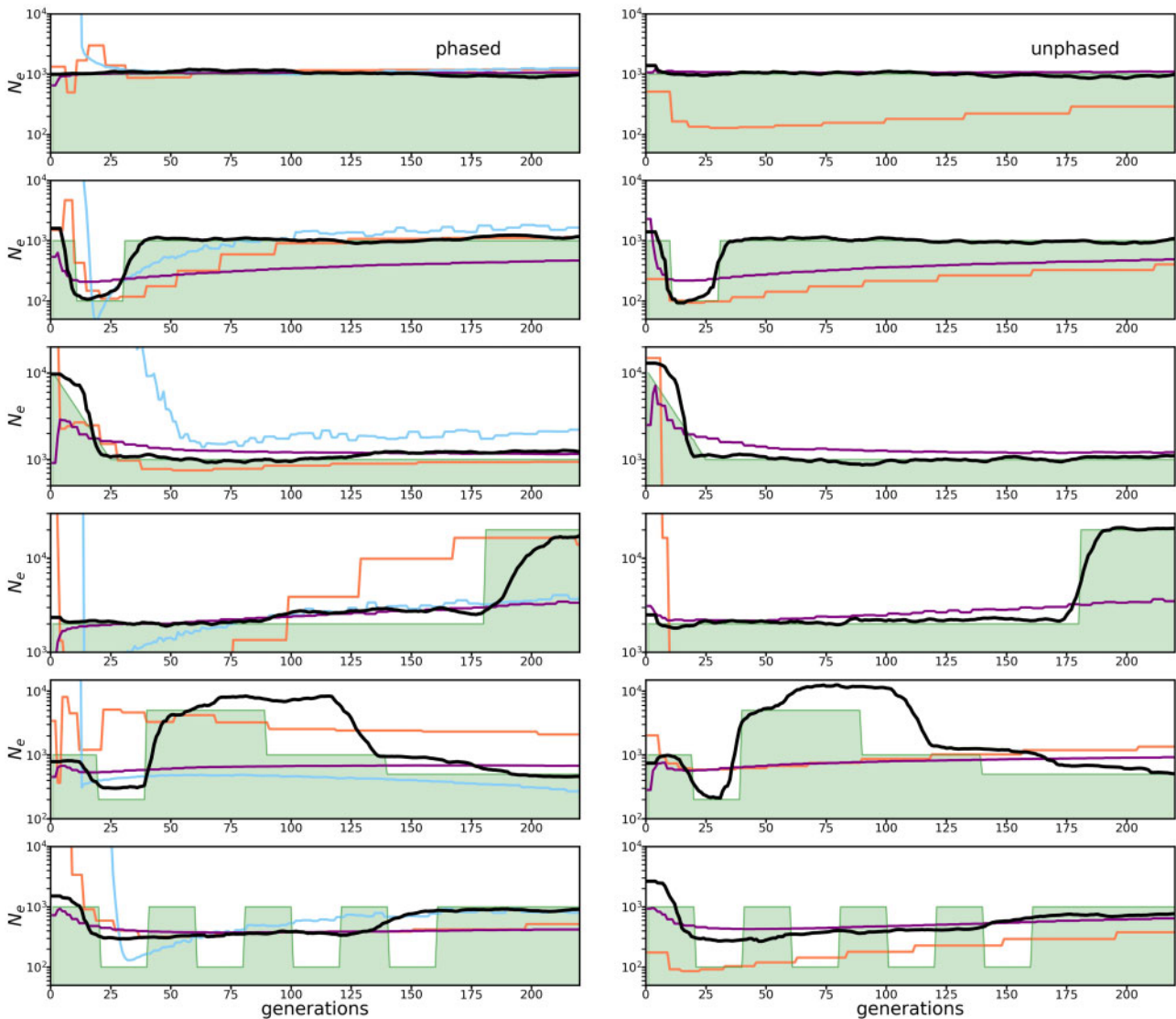
FIG. 1. Estimates of temporal N_e of simulated populations from phased (left) and unphased (right) data under different demographic scenarios from present (generation 0) to 220 generations in the past. The green area is the true (simulated) population size. The black, orange, blue, and purple lines are, respectively, estimations by GONE, MSMC, Relate (only for phased data) and by using the equations of the LinkNe software. Samples were composed of four diploid individuals (eight haplotypes) for MSMC and 20 diploid individuals for the other methods. The total number of SNPs involved in the estimations ranged between 255,000 and 450,000 depending on the scenarios. No MAF threshold was applied to the data.

differences are mitigated if data from distant loci (say $c > 0.05$) are not included in the analysis, leading to more consistent estimations (fig. 2J).

Application to Real Data

We next apply the method to infer recent demographic changes of several human and animal populations (fig. 3) with large differences in size. In order to reduce the effect of sampling on estimates for recent generations observed in simulations, LD data for recombination rates >0.05 were excluded from the analysis. Inferences of N_e from a herd of domestic pigs, which was founded from populations of unknown origins and then maintained under controlled mating conditions for 26 generations before sampling, are in agreement with estimates obtained from the observed genealogical

information of individuals (Saura et al. 2015) except for generations close to the setup of the population. This deviation is exactly the kind of artifact expected after mixing different populations as shown by simulations (fig. 2D).

The estimated small N_e values in pigs contrast with the large recent N_e values inferred from a sample of 99 individuals from the Finnish population, which has experienced a rapid growth during the last 20 generations. In this case, the data were obtained from a sequencing analysis and a large number of SNPs (>9 million) were available. Thus, we made 20 replicate analyses, each having 50,000 SNPs sampled randomly from each chromosome. The red thick line is the average over replicates and the shadow area gives the interval of confidence obtained from the replicates. These estimations show some differences with a previous study based on the analysis
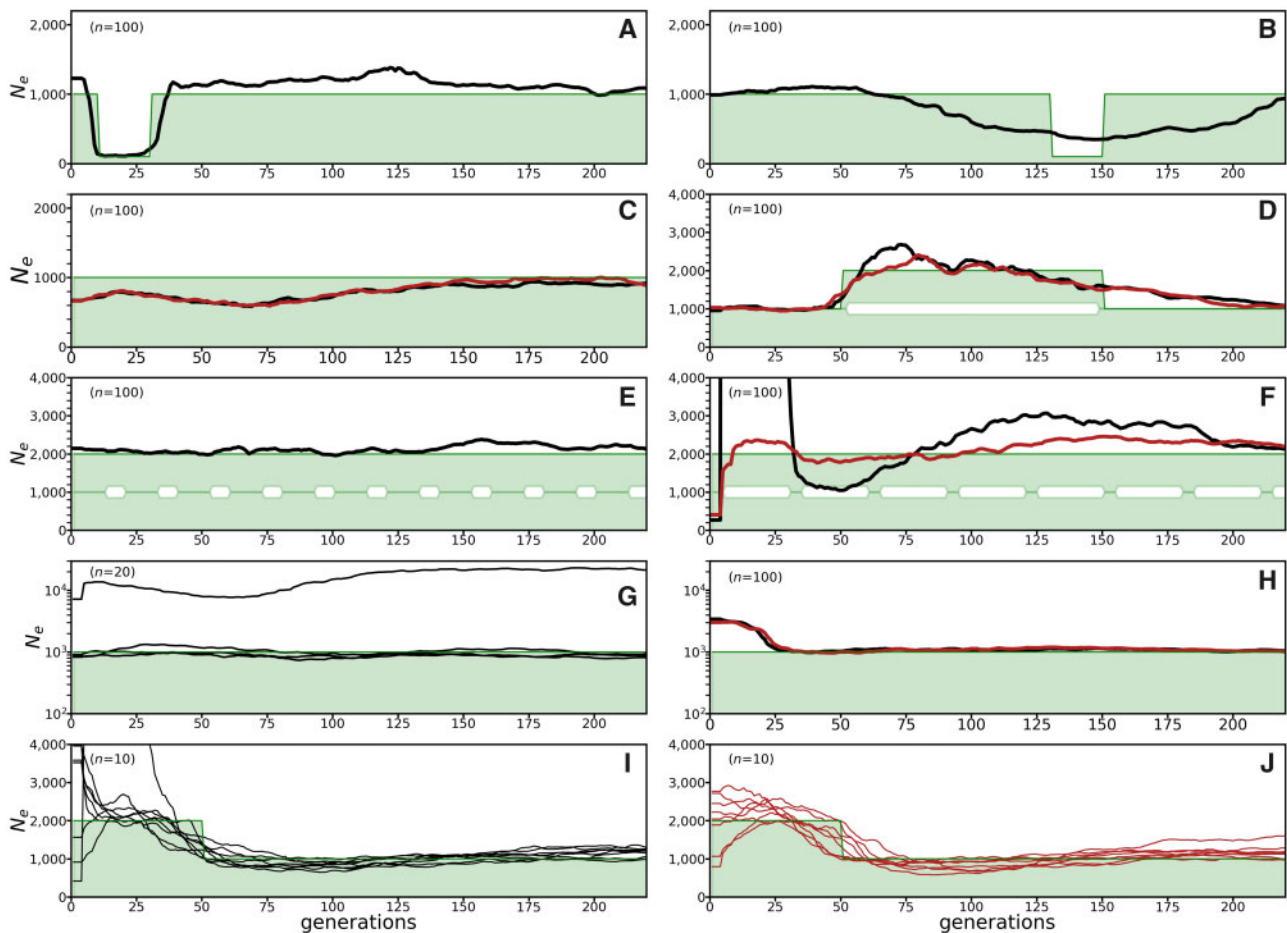
Fig. 2. Estimates of temporal N_e by GONE under different simulated demographic scenarios from present (generation 0) to 220 generations in the past. The true population size is the green shadowed area and n is the sample size of individuals for analysis. For all panels, the black lines refer to an analysis where all recombination bins from $c = 0.001$ up to $c = 0.5$ are considered (option $hc = 0.5$), whereas the red lines refer to analyses with rate bins from $c = 0.001$ up to only 0.05 ($hc = 0.05$). (A) and (B) Detection of bottlenecks occurring at different times. (C) Scenario with overlapping generations with three cohorts per generation and mixed-cohort sampling. (D) A population $N_e = 1,000$ was divided into two populations $N_e = 1,000$ each, which were isolated for 100 generations and then mixed 50 generations ago into a single population with $N_e = 1,000$. (E) and (F) Metapopulation composed of two subpopulations $N_e = 1,000$ each with 2% and 0.2% of migration, respectively, between them. (G) Estimations under different base-calling error rates. From top to bottom, 10%, 1%, 0.1% and 0%, the latter two being indistinguishable. (H) A hundred individuals were sampled from the population over a period of 100 consecutive generations at a rate of one sampled individual per generation. (I) and (J) Eight small samples ($n = 10$ each) were taken from the same population at the same time.

of IBD segments of a much larger sample of 5,402 individuals (Browning and Browning 2015). Although the IBD inference assumed a monotonic increase of population size, we detect a reduction in the Finnish population during the middle ages, which could be in fact a result of the admixture of partially differentiated populations in iron age and medieval times (Översti et al. 2019). Our estimations for recent times are clearly under the actual numbers of Finns. This deviation can only be partially explained by the substantial differences between effective sizes (N_e) and census sizes (N) generally observed in natural populations. Additionally, the figure shows that the use of an alternative map with constant recombination rate of 1.2 cM/Mb across the genome (green continuous line) does not make a big difference in the estimations of demography of the Finnish population.

The analyses of salmon samples composed by individuals born between 1985 and 1992 from two tributaries of River Dee in Scotland highlight the consistency of the method

when applied to replicate samples. Both estimates are coincident with a drop in population size about ten generations before sampling. Although fine-scale recombination maps were used for pigs and humans, this salmon analysis assumes a constant rate of recombination of 1 cM/Mb for the whole genome, which is an approximated average of estimates by several authors (Phillips et al. 2009; Lien et al. 2011; Tsai et al. 2016). Salmon genome underwent a recent event of diploidization and several chromosome rearrangements (Lien et al. 2016) and is still polymorphic for some of them. Consequently, there is a lack of continuity between the assumed physical and the estimated genetic maps but, by removing loci pairs with large recombination rates (over $c = 0.05$ in this analysis), we avoid most complications due to gaps or lacks of continuity.

Analysis of samples of ancient human remains dated between 2,500 and 4,500 years BCE (Olalde et al. 2018) produces N_e estimates between 2,000 and 6,000 individuals from two
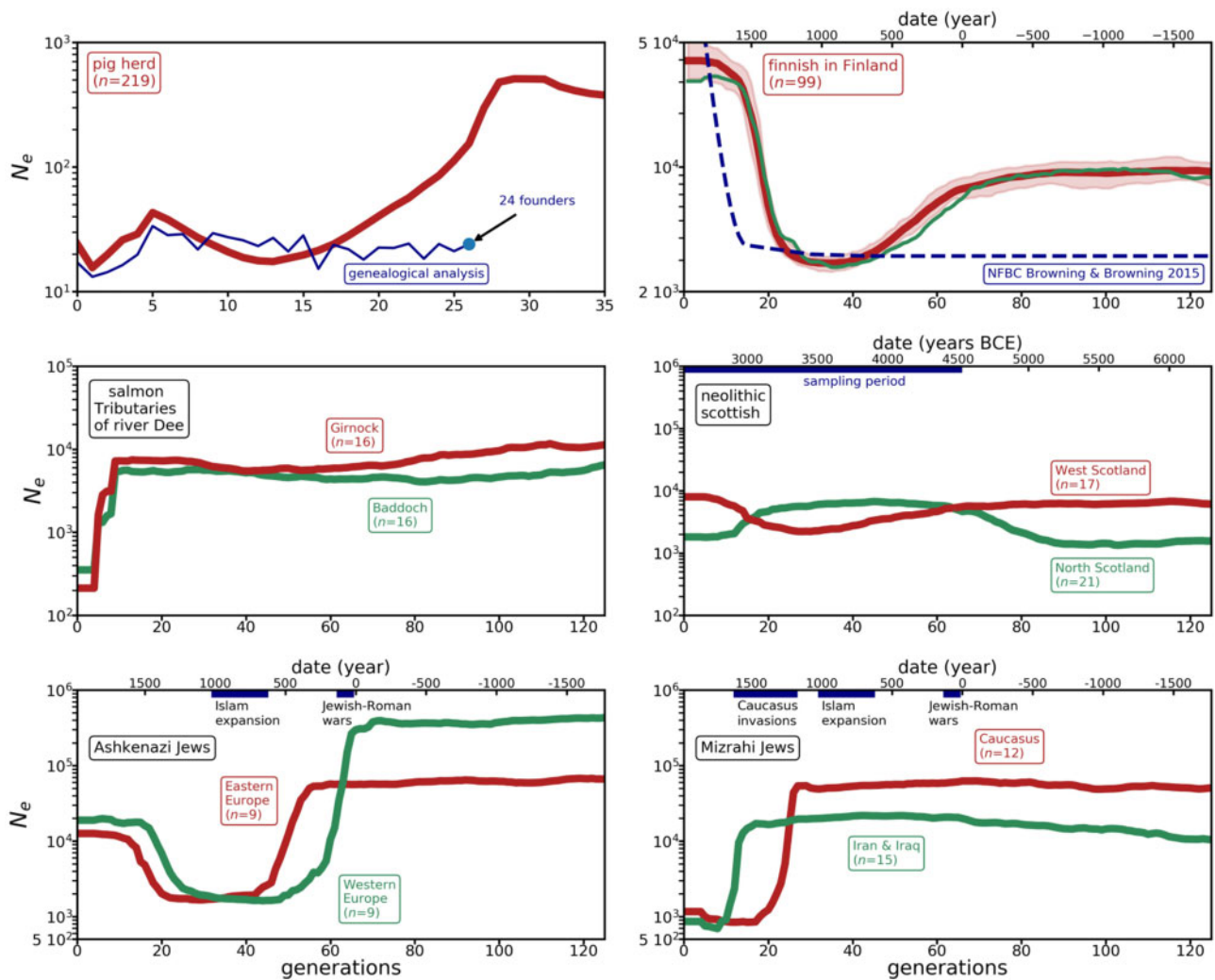
FIG. 3. Estimates of temporal N_e of real populations with different sample sizes (n). PIGS: Guadyerbas population of Iberian pigs. The thin blue line is the estimate of N_e using the individual contributions from genealogical data (Saura et al. 2015). FINNISH: Estimates of Finnish human population. The shadow area gives the 90% confidence interval of the estimates obtained by running 20 replicates, each one corresponding to a random sample of 50,000 SNPs for each chromosome. The thin broken blue line is the estimation obtained by Browning and Browning (2015) for a Northern Finnish NFBC sample of 5,402 individuals. The thin green line is the estimate of N_e assuming a constant recombination rate of 1.2 cM/Mb. SALMON DEE: Atlantic salmons of two tributaries of River Dee in Scotland. NEOLITHIC: Two neolithic samples from West and North Scotland, where the sampling period accounts for about 60 generations. ASHKENAZI JEWS: Samples of eastern and western European populations. MIZRAHI JEWS: Samples from a Caucasus population and from Iran and Iraq. All estimations assume no MAF threshold and unphased genomes except for the NEOLITHIC, which involves pseudohaploid genomes.

Scottish samples. The "random draw" method of genotyping of these ancient-DNA samples results in pseudohaploid genomes (Haak et al. 2015). Although other N_e estimators do not perform adequately with this type of data, our method can be straightforwardly modified to accommodate it (Supplementary File, Supplementary Material online). Simulation results accounting for an extended sampling period of 100 generations (fig. 2H) showed estimation bias for about a quarter of the time of sampling. Therefore, most recent N_e estimations from these samples should be considered with caution.

Inferences from two samples of Ashkenazi Jews from Eastern and Western Europe (Behar et al. 2010) show similar N_e trajectories with increased deviations for the most distant generations. The strong reduction in N_e inferred around

generation 60 is approximately contemporary with the Jewish-Roman wars of the 1st century, which are commonly considered to have contributed to the expansion of the Jewish diaspora across Europe, Africa, and Asia (Goodman 2004). The large expansion of this ethnic group in recent times (Slatkin 2004) is not observed in our results, which only show a moderate increase. This, again, illustrates the difficulties of the method in detecting large increases of N_e in recent times from very small samples. The analysis of Mizrahi genomes does not show any decline in N_e at generation 60, which is coincident with the fact that these communities were included in the Parthian Empire by that time and were not affected by the Jewish-Roman wars (Goodman 2004). No significant effect of the later expansion of Islam on N_e is observed but a sharp drop in N_e is detected particularly

in Caucasian Mizrahim, which is coincident with the repeated invasions of the region between the 13th and 16th centuries (Singer 1906), and a later decline is observed in Mizrahi Jews from Iran and Iraq.

Discussion

Our method is able to infer demographic histories within a hundred generations in the past from both phased and unphased genotypes. These short-term inferences appear to be more accurate than those obtained by current coalescence methods and LD-based methods ignoring the cumulative drift effects. The mapping of mutations to estimate the length of branches of genealogical trees makes coalescence theory rather more suitable for modeling ancient demography because mutations accumulate very slowly in populations. Consequently, estimations from coalescence methods deviate from the real N_e for recent generations, as can be observed for Relate estimations from simulated data (fig. 1). On the contrary, MSMC makes use of the observed changes in heterozygosity across the genome to infer demography, which considers both mutation and recombination events. Although MSMC performs better than Relate, it lacks enough power to resolve recent demographic changes. The reason is probably because few recombination events between consecutive sites are dated in recent times even when eight haplotypes are included in the sample. The inclusion of more haplotypes could improve the recent N_e estimates but the method would probably become computationally intractable.

GONE makes use of the information from a wide range of recombination rates, including distant loci for which at least one crossover event is expected in every meiosis. Every new mutation generates a small amount of LD between the mutation site and any other polymorphic site. This LD is expected to increase by genetic drift over consecutive generations at a rate which depends on N_e, and to decrease by recombination over generations at a rate which depends on the genetic distance between loci. Thus, the observed LD between distant loci is mainly the result of the recent drift because the effect of old drift is removed by intense recombination in a few generations, whereas LD between closely linked loci is the result of drift generated both recently and remotely in the past (Hayes et al. 2003).

Relevant aspects of GONE allow the detection of demographic changes in scenarios where previous LD methods fail. One of them is the use of δ^2 (Ohta and Kimura 1969) to measure LD instead of the generally used Pearson's r. The use of r^2 to infer temporal changes of N_e is problematic, as there are no analytic solutions for its sampling error. This makes difficult to reach accurate predictions of the cumulative effects of drift on LD over generations, particularly when the recombination rate is small. The general approximation by Fisher (1915) for the normal distribution and some related variations (Tenesa et al. 2007) are inaccurate for a bivariate binomial distribution, for which r^2 depends on gene frequencies in an intricate way. On the contrary, δ^2 is the ratio of two statistics whose expectations in consecutive generations can

be established. In addition, because δ^2 is a measure of LD weighted by the genetic variances of the involved loci (Rogers 2014), it is much less affected than r^2 by sampling of low-frequency variants and by genotyping errors, which usually generate singleton variants in samples. Methods using r^2 (Tenesa et al. 2007; Saura et al. 2015; Mörseburg et al. 2016) are prone to overestimations of N_e under those circumstances, which are partially corrected by applying an arbitrary MAF threshold to data (supplementary fig. S1, Supplementary Material online). For our method, however, the application of MAF thresholds generally results in slightly biased estimates of N_e and should not be applied a priori, except when DNA sequencing generates low-quality data. In this context, the application of MAF thresholds results in acceptable N_e estimates except when the rate of base-calling errors is very high ($\sim$10% or higher) (fig. 2G). We have derived accurate and computationally efficient equations to predict the change of δ^2 over consecutive generations. This accuracy is critical because the inference of N_e across time is the result of the comparison of the accumulated contributions of all previous generations to the observed δ^2 values for pairs of loci with different recombination rates. We also derived appropriate corrections for sampling, some of them similar but more accurate than previous developments, and extended them to new sampling methods.

Several authors derived solutions for the expected value of δ^2 (Ohta and Kimura 1971; Hill 1975; Weir and Hill 1980; McVean 2007). Recently Ragsdale and Gravel (2020) developed a combinatorial method to find estimators of several statistics related with δ^2, which were combined with the predictive theory by Hill and Robertson (1968) in order to consider sampling-without-replacement in the genetic transition of a population from one generation to the next one. Their predictions of LD at equilibrium when $c = 0.5$ and population size is constant over time were $\delta^2 = 1/(6N)$ for haploids and $\delta^2 = 1/(3N)$ for diploids, the latter being also obtained by Weir and Hill (1980). However, for $c = 0.5$, our results are $\delta^2 \approx 2/(3N)$ and $5/(6N)$ for haploids and diploids, respectively, which are in agreement with the statistical concept that the expected values of δ^2 and r^2 in a random sample of size $2N$ cannot be smaller than $1/(2N)$ (Section 4 of Supplementary File, Supplementary Material online). Simulations show that our predictions of δ^2 with constant population size are more accurate for the whole range of recombination rates than those predicted by previous theory (supplementary table S1, Supplementary Material online).

As we have explained above, the expected LD for a particular recombination rate is not the consequence of drift (N_e) at a particular generation, but the consequence of drift accumulated over many generations in the past. Previous two-loci LD-based methods (Hayes et al. 2003; Tenesa et al. 2007; Barbato et al. 2015; Mezzavilla and Ghiroto 2015; Hollenbeck et al. 2016) assume a univocal correspondence between N_e at a particular generation g in the past and the observed LD between pairs of loci with a particular recombination rate $c = 1/(2g)$. This relationship was deduced by Hayes et al. (2003) in the context of the probability that

two chromosome segments, which are flanked by two markers with recombination rate c, come from a common ancestor without intervening recombination. As stated by Hayes et al. (2003), this approach would be only valid for constant N_e or a linear increment or decrement of N_e across generations. Our method, however, provides a solution for the inference of the historical N_e without any previous assumption on the magnitude or the trend of changes. In addition, the method is quite robust for base-calling errors, deviations for the genetic map, and deviations from the assumption of a single unstructured population. Overlapping generations tend to produce underestimations of the recent N_e, as has been reported for the estimations of the current N_e (Waples et al. 2014). In addition, although the admixture of differentiated populations distorts the structure of LD, inferences are valid for the derived population up to nearly the generation of admixture.

Although all bins for pairs of SNPs at different distances can be used in the estimation procedure, it is advised in practice to ignore those corresponding to the largest recombination frequencies and consequently the default largest value of c used in our application is set to 0.05. The reasons for this are 3-fold. First, random sampling of few individuals can lead to deviations from the average coancestry of the population (fig. 2I). The consequences of these deviations on the inference of temporal N_e are larger for large c values than for small ones because genealogies of a finite sample of individuals mix progressively with the population going backward in time. That is, inferences of recent N_e are more affected by sampling than inferences of ancient N_e. These biases are partially corrected by disregarding large values of c (cf. fig. 2I and J). Second, the observed LD for any particular c value does not depend exclusively on the N_e at a particular generation back in time. However, although LD of SNP pairs with $c = 0.5$ depends on the N_e of a few recent generations (say a couple generations back in time), LD of bins with smaller c values depends on the historical N_e values of a wider span of time from past to present, including the recent generations. As the inferences of N_e at different generations are interconnected in this way, biases in the measure of LD of bins with large c values affect more the inference of the whole series of temporal N_e than biases of LD of small c values do. Finally, when populations are strongly geographically structured, the distortion in LD can be very large (fig. 2F). This effect is relatively similar to the random sampling of a few individuals in a panmictic population. By ignoring bins of large c values, the distortion in the inference of past N_e is mitigated. Nevertheless, our recommendation of considering the largest value c as 0.05 is a compromise solution which can be changed by the user by setting the switch of this option to any other value between 0 and 0.5. For example, for simulation results, where the sampling of individuals is a random sample of the population, the use of the largest c values is justified unless the sample size is very small.

Inferences by GONE are restricted to recent changes in N_e, with the highest resolution within a hundred generations before sampling. Drastic demographic changes partially erase the LD footprint of older events. Therefore, if older changes are relatively small or there are many demographic changes involved in the time period considered, the method will fail to detect them accurately or will only detect the most recent ones. The lack of precision of N_e estimates of ancient events (fig. 2A vs. 2B) could be a consequence of the fact that ancient N_e estimates rely on a large number of measures of LD of different recombination-rate bins. Thus, cumulative errors are expected to be larger for ancient estimates than for recent ones.

To a good approximation, the accuracy of the estimations is proportional to the sample size, to the squared root of the number of pairs of SNPs included in the analysis and to the inverse of the effective population size (see methods and Section 11 of Supplementary File, Supplementary Material online). That is, halving the sample size can be approximately compensated by doubling the number of SNPs included in the analysis. This is consistent with previous findings related to N_e estimation by the temporal method (Waples 1989). Note, however, that this approximation relies on the assumption that the individuals analyzed are a truly random sample from the population. Even so, if the sample size is very small, the accuracy of population parameter estimates cannot be compensated by a larger number of SNPs. As noted by King et al. (2018), with more and more loci the estimates converge on the true parameter values for the pedigree of the sampled individuals, but not necessarily on the pedigree of the population as a whole. For deep coalescent evaluations this is not such a big problem, as all recent pedigrees coalesce to the same ancestral lineages as one moves back in time. However, this is an important issue for recent generations, particularly in large populations, because the drift signal (proportional to $1/N$) is weak and a large sample size n is required in order to be detected, as sampling error is proportional to $1/n$.

Here, we have introduced a method to infer very recent changes in effective population size from the distribution of LD between pairs of SNPs from chip genotyping or DNA sequencing data. Its temporal space of inference is of particular interest in the survey and assessment of perspectives of endangered populations and could also be a useful historiographic tool to study human demography. It is computationally efficient, accurate, and fairly stable against deviations from the assumptions of the model such as genotyping errors, nonrandom mating, admixture of populations, overlapping generations, and alterations of the genetic map. It is applicable to populations with a wide range of demographic changes and different types of genomic data. In summary, this method facilitates the immediate use of a large amount of genomic information to study the recent demography of populations.

Materials and Methods

Estimation of the Historical N_e

In a first step, SNP data files with *map* and *ped* formats are processed by a custom program to calculate LD (sample d_c^2) for bins of pairs of SNPs with different recombination rates (c). The analysis is made for individual chromosomes, which can be run in parallel on several processors. It has a number of options: 1) the number and length of bins assumed; 2) the use

of the observed genetic distances between SNPs, if available in the *map* file, or the use of genetic distances calculated under the assumption of a given number of cM/Mb of sequence; 3) the use of Haldane's or Kosambi's corrections for genetic distances, or none of them; 4) the exclusion or inclusion of SNPs with missing data; 5) the use of phased diploid data, unphased diploid data, or pseudohaploid data; 6) a predefined maximum number of SNPs to be analyzed per chromosome, taken at random among all available SNPs, and excluding loci with more than two alleles; and 7) the application of a threshold MAF if desired. Values of d_c^2 from all chromosomes are then combined in a single file for estimation of historical series of N_e, although estimates from individual chromosomes can also be performed.

A second program (GONE) implements a genetic algorithm (Mitchell 1998) to search for the global optimal solution of the historical N_e series that best fits the observed δ_c^2 values. The function to be minimized is the sum of the squared differences between observed and predicted δ_c^2 values for the whole range of recombination rates c considered in the analysis. In this genetic algorithm, an "individual" is a particular sequence of temporal N_e values for all the previous generations. In order to reduce the complexity of the optimization procedure, the entire time space from 0 (i.e., at the sampling point) to an infinite number of generations in the past is split into consecutive blocks, with the same N_e value for all the generations within each block. In order to generate each initial "individual," the time space is randomly split into four blocks with a boundary set at generation $1/c_{min}$, where c_{min} is the minimum c value among all pairs of SNPs included in the analysis, and random N_e values are assigned to each block. Thus, 1,000 "individuals" are randomly generated and fitness values are assigned as the inverse of the sum over c bins of the squared differences between observed and predicted δ_c^2 values calculated from the set of N_e values of the "individual." Then, the fittest 100 "individuals" are selected to be "parents" of the next "generation." In order to produce each "individual" of the next "generation," two "parents" are randomly selected, "crossovers" (interchange of sections of temporal N_e series) between both "parents" are carried out and "mutations" (changes in the boundaries of blocks and the N_e values of blocks) occur randomly. Each "crossover" introduces a new boundary, but the number of blocks can also be reduced by random "mutations" that merge two consecutive blocks. In this way, a new set of 1,000 "individuals" is generated and selection of "parents" starts again to produce the next "generation." The block from generation $1/c_{min}$ up to infinity will remain without further divisions during the whole optimization. The selective process is repeated for 750 "generations" and the average N_e series of the best ten "individuals" is considered to be the solution of the optimization process. As this solution could be an "adaptive peak", that is a local optimal solution, the "selective process" is repeated a desired number of times (say 40) and the final solution is calculated as the average value of the available solutions, for example, $40 \times 10 = 400$ "individuals." The replicated estimations can also be run in parallel using several processors. Thus, GONE provides a

solution of consensus trend for the demographic history of a population with two output files: the estimate of the temporal N_e series (Output_Ne_* file) and the series of observed and predicted d_c^2 values across the range of recombination rates considered in the analysis (Output_d2_* file). We found that this solution is more consistent and repeatable than other optimization methods, such as simulated annealing. An example of the fit between optimized (estimated) values of d_c^2 and the observed simulated values is given in supplementary figure S2, Supplementary Material online.

The method does not generate parametric confidence intervals for the estimate. However, if the number of SNPs per chromosome is large, which is the case with sequencing data or with some large chips, it is possible to estimate the uncertainty by choosing different sets of SNPs per chromosome using a functionality implemented in the scripts, as mentioned above. This would allow empirical confidence limits to be obtained. An example of this application is shown in figure 3 for the Finnish population. However, confidence intervals calculated in this way should be taken with caution as they do not consider the additional random effect of pedigree sampling in the population when only a small set of individuals are analyzed. An alternative, if the number of individuals sampled is large enough, is to obtain empirical replicated estimations using subsamples of individuals, what would quantify, at least in part, the random pedigree sampling in the population.

Simulation Programs

To check the accuracy and statistical properties of the new LD-based N_e estimation method, simulations were performed with the software SLiM (Messer 2013; Haller and Messer 2019), a forward simulator of SNPs, as well as with in-house programs mainly to check accuracy at particular recombination rates. For most cases, sequences of 250 Mb of length were run for 10,000 generations assuming absence of selection under different demographic scenarios (changes in N over generations), such as bottlenecks, drops, or expansions of the population within the last 200 generations. Mutation and recombination rates per nucleotide were assumed to be $\mu = c = 10^{-8}$, which implies 1 Mb = 1 cM. At the last generation, a sample of n diploid individuals (20 or 100) without replacement was taken for analysis. We also considered sampling with replacement in some cases to check the corresponding estimations under this sampling scenario. In general, no pruning was made regarding MAF, but some simulations were run by applying MAF <0.05 and 0.1 to check the effects of rare alleles. Simulation results were based on 10–100 replicates for each scenario. A custom program was used to obtain the *map* and *ped* files needed to start the estimation procedure.

Estimation of Temporal N_e with Other Methods

The *map* and *ped* files of a number of simulated scenarios were transformed into the necessary file formats for MSMC (Schiffels and Durbin 2014) and Relate (Speidel et al. 2019) and parameters were set to the default options. Analyses of unphased genotypes were implemented by indicating all the

possible phasing modes in MSMC. Likewise, the d_c^2 values obtained in the simulations were analyzed by previous estimators of temporal N_e with LD (Tenesa et al. 2007; Barbato et al. 2015; Mezzavilla and Ghiroto 2015; Hollenbeck et al. 2016) with the corresponding corrections for phased and unphased genotypes.

Sample Size Estimation

By assuming some simplifications (Section 11 of Supplementary File, Supplementary Material online), it can be shown that the power of detecting fluctuations in N_e is roughly proportional to:

$$G = \frac{n \cdot \sqrt{\vartheta}}{N_e},$$

where n is the sample size and ϑ is the number of loci pairs included in the analysis. As a general rule for experiments in which the range of c values varies from 0.5 to 0.001, good estimations of effective population sizes are obtained when $G > 100$ and very poor estimations are obtained when $G < 10$.

Generation Time

In order to compare inferences of N_e with references to historical events, generation time was set to 30 years for humans (Fenner 2005).

Relationship between Physical and Recombination Maps

A genetic map in centi-Morgans (cM) and a map function are needed to estimate the recombination frequency c between any pair of loci from their physical positions in the genome. A fine-scale recombination map was used for humans (Myers et al. 2005) and an inferred map from data by Tortereau et al. (2012) was used for pigs.

There is not a consensus on physical and genetic maps to date for salmon, probably due to the complexity of the chromosome rearrangements in this species. We used the salmon reference genome assembly ICSASG_v2 (Lien et al. 2011) to assign locations to SNPs and considered a constant ratio of 1 cM/Mb for the relationship between genetic and physical maps, which is an approximate average over several studies (Phillips et al. 2009; Lien et al. 2011; Tsai et al. 2016). Tsai et al. (2016) showed the lack of continuity between the assumed physical and the estimated genetic maps, particularly for some chromosomes, with gaps of up to 150 cM. However, by ignoring recombination rates over 0.05 (with the option hc 0.05) we avoided most complications due to gaps or lacks of continuity in the genome. Note that, at 1 cM/Mb, a recombination rate of 0.05 corresponds to 5.3 Mb assuming Haldane's function. Using SNPs closer than this distance makes improbable to have a significant representation of SNP pairs at different sides of a gap.

Samples

The different sample sizes of individuals analyzed (n) and the number of SNPs (N_{SNP}) analyzed in the estimations are as follows. Guadyerbas population of Iberian pig (Saura et al. 2015) ($n = 219$; $N_{SNP} = 19,144$), Finnish population (1000 Genomes Project Consortium 2012; last accessed March 27, 2017) ($n = 99$; $N_{SNP} = 1,100,000$), Salmon from River Dee ($n = 16$ for each population; $N_{SNP} = 104,354$), Neolithic West Scotland (Olalde et al. 2018) ($n = 17$ [10.8], where the number in brackets refers to the actual sample size disregarding missing genotyping data; $N_{SNP} = 552,191$), Neolithic North Scotland (Olalde et al. 2018) ($n = 21$ [14.8]; $N_{SNP} = 594,385$), Ashkenazi East (Behar et al. 2010) ($n = 9$; $N_{SNP} = 478,394$), Ashkenazi West (Behar et al. 2010) ($n = 9$; $N_{SNP} = 477,884$), Mizrahim from Caucasus (Behar et al. 2010) ($n = 12$; $N_{SNP} = 486,075$), Mizrahim from Iran and Iraq (Behar et al. 2010) ($n = 15$; $N_{SNP} = 485,199$).

Software Availability

The scripts and programs (Linux and MacOSX) necessary to apply the method are available at GitHub address https://github.com/esrud/GONE.

Supplementary Material

Supplementary data are available at *Molecular Biology and Evolution* online.

Author Contributions

E.S. and A.C. conceived the work and wrote the article. E.S. developed the theory and the computational solution. A.C. designed the structure of data and the analysis. I.N. compared methods. A.F.P. contributed human data and investigations. M.S. contributed animal data and analysis. J.W. provided intellectual input.

References

1000 Genomes Project Consortium. 2012. An integrated map of genetic variation from 1,092 human genomes. *Nature* 491:56–65 (last accessed March 27, 2017).

Atkinson QD, Gray RD, Drummond AJ. 2008. mtDNA variation predicts population size in humans and reveals a major Southern Asian chapter in human prehistory. Mol Biol Evol. 25(2):468–474.

Barbato M, Orozco-terWengel P, Tapio M, Bruford MW. 2015. SNeP: a tool to estimate trends in recent effective population size trajectories using genome-wide SNP data. Front Genet. 6:109.

Behar DM, Yunusbayev B, Metspalu M, Metspalu E, Rosset S, Parik J, Rootsi S, Chaubey G, Kutuev I, Yudkovsky G, et al. 2010. The genome-wide structure of the Jewish people. Nature 466(7303):238–242.

Browning SR, Browning BL. 2015. Accurate non-parametric estimation of recent effective population size from segments of identity by descent. Am J Hum Genet. 97(3):404–418.

Corbin LJ, Liu AYH, Bishop SC, Woolliams JA. 2012. Estimation of historical effective population size using linkage disequilibria with marker data. J Anim Breed Genet. 129(4):257–270.

Fenner JN. 2005. Cross-cultural estimation of the human generation interval for use in genetics-based population divergence studies. Am J Phys Anthropol. 128(2):415–423.

Fisher RA. 1915. Frequency distribution of the values of the correlation coefficient in samples from an indefinitely large population. Biometrika 10(4):507–521.

Goodman M. 2004. Trajan and the origins of Roman hostility to the Jews. Past Present. 182(1):3–29.

Haak W, Lazaridis I, Patterson N, Rohland N, Mallick S, Llamas B, Brandt G, Nordenfelt S, Harney E, Stewardson K, et al. 2015. Massive migration from the steppe was a source for Indo-European languages in Europe. Nature 522(7555):207–211.

Haller BC, Messer PW. 2019. SLiM 3: forward genetic simulations beyond the Wright-Fisher model. Mol Biol Evol. 36(3):632–637.

Hayes BJ, Visscher PM, McPartlan HC, Goddard ME. 2003. Novel multi-locus measure of linkage disequilibrium to estimate past effective population size. Genome Res. 13(4):635–643.

Hill WG. 1975. Linkage disequilibrium among multiple neutral alleles produced by mutation in finite populations. Theor Pop Biol. 8(2):117–126.

Hill WG, Robertson A. 1968. Linkage disequilibrium in finite populations. Theor Appl Genet. 38(6):226–231.

Hollenbeck CM, Portnoy DS, Gold JR. 2016. A method for detecting recent changes in contemporary effective population size from linkage disequilibrium at linked and unlinked loci. Heredity 117(4):207–216.

Hudson RR. 1990. Gene genealogies and the coalescent process. Oxf Surv Evol Biol. 7:1–44.

King L, Wakeley J, Carmi S. 2018. A non-zero variance of Tajima's estimator for two sequences even for infinitely many unlinked loci. Theor Popul Biol. 122:22–29.

Li H, Durbin R. 2011. Inference of human population history from individual whole-genome sequences. Nature 475(7357):493–496.

Lien S, Gidskehaug L, Moen T, Hayes BJ, Berg PR, Davidson WS, Omholt SW, Kent MP. 2011. A dense SNP-based linkage map for Atlantic salmon (Salmo salar) reveals extended chromosome homeologies and striking differences in sex-specific recombination patterns. BMC Genomics 12:615.

Lien S, Koop BF, Sandve SR, Miller JR, Kent MP, Nome T, Hvidsten TR, Leong JS, Minkley DR, Zimin A, et al. 2016. The Atlantic salmon genome provides unsights into rediploidization. Nature 533(7602):200–205.

McVean G. 2007. A genealogical interpretation of linkage disequilibrium. Genetics 175(3):1395–1991.

Messer P. 2013. SLiM: simulating evolution with selection and linkage. Genetics 194(4):1037–1039.

Mezzavilla M, Ghiroto S. 2015. Neon: an R package to estimate human effective population size and divergence time from patterns of linkage disequilibrium between SNPS. J Comput Sci Syst Biol. 8(1):

Mitchell M. 1998. An introduction to genetic algorithms. Cambridge: MIT Press.

Mörseburg A, Pagani L, Ricaut F-X, Yngvadottir B, Harney E, Castillo C, Hoogervorst T, Antao T, Kusuma P, Brucato N, et al. 2016. Multi-layered population structure in island Southeast Asians. Eur J Hum Genet. 24(11):1605–1611.

Myers S, Bottolo L, Freeman C, McVean G, Donnelly P. 2005. A fine-scale map of recombination rates and hotspots across the human genome. Science 310(5746):321–324.

Ohta T, Kimura M. 1969. Linkage disequilibrium due to random genetic drift. Genet Res. 13(1):47–55.

Ohta T, Kimura M. 1971. Linkage disequilibrium between two segregating nucleotide sites under the steady flux of mutations in a finite population. Genetics 68:571–580.

Olalde I, Brace S, Allentoft ME, Armit I, Kristiansen K, Booth T, Rohland N, Mallick S, Szécsényi-Nagy A, Mittnik A, et al. 2018. The beaker phenomenon and the genomic transformation of Northwest Europe. Nature 555(7695):190–196.

Översti S, Majander K, Salmela E, Salo K, Arppe L, Belskiy S, Etu-Sihvola H, Laakso V, Mikkola E, Pfrengle S, et al. 2019. Human mitochondrial DNA lineages in Iron-Age Fennoscandia suggest incipient admixture and eastern introduction of farming-related maternal ancestry. Sci Rep. 9(1):16883.

Palacios JA, Wakeley J, Ramachandran S. 2015. Bayesian nonparametric inference of population size changes from sequential genealogies. Genetics 201(1):281–304.

Palamara PF, Lencz T, Darvasi A, Pe'er I. 2012. Length distributions of identity by descent reveal fine-scale demographic history. Am J Hum Genet. 91(5):809–822.

Phillips RB, Keatley KA, Morasch MR, Ventura AB, Lubieniecki KP, Koop BF, Danzmann RG, Davidson WS. 2009. Assignment of Atlantic salmon (Salmo salar) linkage groups to specific chromosomes: conservation of large syntenic blocks corresponding to whole chromosome arms in rainbow trout (Oncorhynchus mykiss). BMC Genet. 10(1):46.

Qanbari S, Pimentel EGC, Tetens J, Thaller G, Lichtner P, Sharifi AR, Simianer H. 2010. The pattern of linkage disequilibrium in German Holstein cattle. Anim Genet. 41:346–356.

Ragsdale A, Gravel S. 2020. Unbiased estimation of linkage disequilibrium from unphased data. Mol Biol Evol. 37(3):923–932.

Ragsdale AP, Gutenkunst RN. 2017. Inferring demographic history using two-locus statistics. Genetics 206(2):1037–1048.

Rogers A. 2014. How population growth affects linkage disequilibrium. Genetics 197(4):1329–1341.

Saura M, Tenesa A, Woolliams JA, Fernández A, Villanueva B. 2015. Evaluation of the linkage-disequilibrium method for the estimation of effective population size when generations overlap: an empirical case. BMC Genomics 16:922.

Schiffels S, Durbin R. 2014. Inferring human population size and separation history from multiple genome sequences. Nat Genet. 46(8):919–925.

Singer I, editors. 1906. The Jewish encyclopedia. New York: Funk & Wagnalls.

Slatkin M. 2004. A population-genetic test of founder effects and implications for Ashkenazi Jewish diseases. Am J Hum Genet. 75(2):282–293.

Speidel L, Forest M, Shi S, Myers SR. 2019. A method for genome-wide genealogy estimation for thousands of samples. Nat Genet. 51(9):1321–1329.

Sved JA. 1971. Linkage disequilibrium and homozygosity of chromosome segments in finite population. Theor Popul Biol. 2(2):125–141.

Sved JA, Cameron EC, Gilchrist AS. 2013. Estimating effective population size from linkage disequilibrium between unlinked loci: theory and application to fruit fly outbreak populations. PLoS One 8(7):e69078.

Sved JA, Hill WG. 2018. One hundred years of linkage disequilibrium. Genetics 209(3):629–636.

Tenesa A, Navarro P, Hayes BJ, Duffy DL, Clarke GM, Goddard ME, Visscher PM. 2007. Recent human effective population size estimated from linkage disequilibrium. Genome Res. 17(4):520–526.

Terhorst J, Kamm JA, Song YS. 2017. Robust and scalable inference of population history from hundreds of unphased whole-genomes. Nat Genet. 49(2):303–309.

Tortereau F, Servin B, Frantz L, Megens HJ, Milan D, Rohrer G, Wiedmann R, Beever J, Archibald AL, Schook LB, et al. 2012. A high density recombination map of the pig reveals a correlation between sex-specific recombination and GC content. *BMC Genomics* 13(1):586.

Tsai HY, Robledo D, Lowe NR, Bekaert M, Taggart JB, Bron JE, Houston RD. 2016. Construction and annotation of a high density SNP linkage map of the Atlantic salmon (*Salmo salar*) genome. *G3 (Bethesda)* 6:2173–2179.

Wang J, Santiago E, Caballero A. 2016. Prediction and estimation of effective population size. *Heredity* 117(4):193–206.

Waples RS. 1989. A generalized approach for estimating effective population size from temporal changes in allele frequency. *Genetics* 121(2):379–391.

Waples RS. 2006. A bias correction for estimates of effective population size based on linkage disequilibrium at unlinked gene loci. *Conserv Genet.* 7(2):167–184.

Waples RS, Antao T, Luikart G. 2014. Effects of overlapping generations on linkage disequilibrium estimates o effective population size. *Genetics* 197(2):769–780.

Waples RS, Do C. 2008. LDNE: a program for estimating effective population size from data on linkage disequilibrium. *Mol Ecol Resour.* 8(4):753–756.

Weir BS, Hill WG. 1980. Effect of mating structure on variation in linkage disequilibrium. Genetics 95(2):477–488.